

# Quasinormal modes from potentials surrounding the charged dilaton black hole

Yun Soo Myung<sup>1,a</sup>, Yong-Wan Kim<sup>1,b</sup>, and Young-Jai Park<sup>2,c</sup>

<sup>1</sup>Institute of Basic Science and School of Computer Aided Science,  
Inje University, Gimhae 621-749, Korea

<sup>2</sup>Department of Physics and Center for Quantum Spacetime,  
Sogang University, Seoul 121-742, Korea

## Abstract

We clarify the purely imaginary quasinormal frequencies of a massless scalar perturbation on the 3D charged-dilaton black holes. This case is quite interesting because the potential-step appears outside the event horizon similar to the case of the electromagnetic perturbations on the large Schwarzschild-AdS black holes. It turns out that the potential-step type provides the purely imaginary quasinormal frequencies, while the potential-barrier type gives the complex quasinormal modes.

PACS numbers: 04.70.Dy, 04.60.Kz, 04.30.Nk

Keywords: dilaton, charged black holes, quasinormal modes

<sup>a</sup>ysmyung@inje.ac.kr

<sup>b</sup>ywkim65@gmail.com

<sup>c</sup>yjpark@sogang.ac.kr

# 1 Introduction

The no-hair theorem [1] implies that the external field of a black hole relaxes to a black hole spacetime characterized by three parameters of mass, charge, and angular momentum. In other words, the perturbations left outside the black hole would either be radiated away to infinity or be swallowed by the black hole. This indicates the boundary conditions in asymptotically flat spacetimes: purely outgoing waves at infinity and purely ingoing waves near the event horizon. These boundary conditions for asymptotically AdS spacetimes are changed as no waves at infinity and purely ingoing waves near the event horizon because of the presence of infinitely height potential at infinity. We call the relaxation phase in the dynamics of perturbed black holes as “quasinormal ringing” [2, 3], damped harmonic oscillations with complex frequencies. The perturbation decays and its frequencies are complex since the perturbation field can fall into black hole or radiate to infinity. At late times, all perturbations except a few small modes are radiated away in the similar manner of the last pure dying tones of a ringing bell.

On the other hand, the dynamics of the Schwarzschild black hole perturbations could be represented by the Regge-Wheeler equation by introducing a tortoise coordinate  $r_*$  [4, 5, 6, 7, 8]. This corresponds to the Schrödinger equation, which provides the scattering problem of the perturbation off the potential  $V(r)$  surrounding the event horizon without considering any back-reaction. We have the  $T(\omega)$  transmission and  $R(\omega)$  reflection amplitudes. The greybody factor (absorption cross section) could be obtained using the transmission amplitudes. The quasinormal modes (QNMs) could be read off from the scattering resonances [9]. Specifically, the pole structure of these two amplitudes reflects that the QNMs correspond to purely ingoing modes near the horizon and purely outgoing modes at infinity. In this sense, the potential contains all information on the black hole background.

There had been extensive works done to compute QNMs and to analyze them in various black hole backgrounds [10]. One of the reasons for the attention on QNMs is the conjecture relating anti-de-Sitter space (AdS) and conformal field theory (CFT) [11]. There are many works on AdS black holes on this subject [12, 13, 14, 15, 16]. However, most of the works on QNMs of black holes in four and higher dimensions are numerical except for a few cases [17, 18, 19, 20]. On the other hand, QNMs of the BTZ black hole [21] has been studied with exact results in AdS<sub>3</sub> space [22, 23, 24, 25]. In this case, the black hole corresponds to a thermal state in the CFT<sub>2</sub>, and the

decay of the test perturbation in the black hole spacetime corresponds to the decay of the perturbed state in the  $\text{CFT}_2$ . Actually, the imaginary part of the frequency  $\omega_i$ , which determines how damped the mode, is a measure of the characteristic time  $\tau = 1/\omega_i$  of approach to thermal equilibrium through the  $\text{AdS}_3/\text{CFT}_2$  correspondence.

Recently, the purely imaginary quasinormal frequencies of a massless scalar perturbation on the 3D charged-dilaton black holes (CDBHs) were found using the scattering picture for  $E > V_0$  [26, 27, 28] with the energy  $E = \omega^2$  and the height of the potential-step  $V_0$ . As far as we know, three cases [13, 26, 27, 28] for these quasinormal frequencies including the electromagnetic and odd-gravitational perturbations on the 4D Schwarzschild-AdS (SAdS) black holes are known to date. It seems that as long as the modes are decaying, it does not matter whether they are oscillating or not. However, the purely imaginary quasinormal frequencies represent a special set of modes which are purely damped [16]. These are not regular QNMs because the real part of frequencies vanishes, eliminating the oscillatory behavior of the perturbations which is characteristic of QNMs. In other words, the purely imaginary quasinormal frequencies should be distinguished from the regular QNMs.

Hence, it is very important to explore the connection between the purely imaginary quasinormal frequencies and the potential. Most of potentials surrounding the black holes is the barrier-type localized at  $r_* = 0$  in asymptotically flat spacetimes, whereas most of black holes has monotonically increasing potentials in asymptotically AdS spacetimes. However, the potentials surrounding the CDBH are the step-type, like the potentials surrounding the 4D SAdS black holes for the electromagnetic and odd-gravitational perturbations [13].

In this work, we explore the connection between the quasinormal frequencies and the shape of potentials using the scattering picture for  $E > V_0$ . It turns out that the potential-step type provides the purely imaginary quasinormal frequencies, while the potential-barrier type gives the complex QNMs. On the other hand, for  $E < V_0$  which is the case of de Sitter space [29], we could not find any QNM.

## 2 Potentials surrounding black holes

## 2.1 Potential-step

Let us consider a toy model of wave propagation under a potential-step with a height  $V_0 (< E)$  as shown in Fig. 1. By solving the Schrödinger equation when a wave propagates from right to left, one can easily obtain the incident, reflected, and transmitted flux as

$$\begin{aligned}\mathcal{F}_{in} &= -2\sqrt{\omega^2 - V_0}, \\ \mathcal{F}_{re} &= 2\sqrt{\omega^2 - V_0} |R|^2, \\ \mathcal{F}_{tr} &= -2\omega |T|^2,\end{aligned}\tag{1}$$

respectively, with  $\omega^2 = E$ ,  $\hbar = 1$  and  $m = 1/2$ . Here the  $R$  reflection and  $T$  transmission amplitudes are given by

$$R = \frac{\sqrt{\omega^2 - V_0} - \omega}{\sqrt{\omega^2 - V_0} + \omega}, \quad T = \frac{2\sqrt{\omega^2 - V_0}}{\sqrt{\omega^2 - V_0} + \omega}.\tag{2}$$

Then, the  $r$  reflection and  $t$  transmission coefficients are

$$\begin{aligned}r &= \left| \frac{\mathcal{F}_{re}}{\mathcal{F}_{in}} \right| = \frac{(\sqrt{\omega^2 - V_0} - \omega)^2}{(\sqrt{\omega^2 - V_0} + \omega)^2}, \\ t &= \left| \frac{\mathcal{F}_{tr}}{\mathcal{F}_{in}} \right| = \frac{4\omega\sqrt{\omega^2 - V_0}}{(\sqrt{\omega^2 - V_0} + \omega)^2},\end{aligned}\tag{3}$$

respectively, satisfying with  $r + t = 1$ , which means that the flux are conserved. When the energy of the incident wave increases, the transmission coefficient approaches unity, as shown in Fig. 2. On the other hand, as  $\omega$  approaches  $\sqrt{V_0}$ , one has no transmission and total reflection.

## 2.2 3D charged-dilaton black holes (CDBH)

The starting action with the dilaton field  $\phi$  is given by

$$S = \int d^3x \sqrt{-g} \left[ R + 2e^{4\phi} \Lambda - 4(\nabla\phi)^2 - e^{-4\phi} F_{\mu\nu} F^{\mu\nu} \right]\tag{4}$$

with the cosmological constant  $\Lambda > 0$  for anti-de Sitter spacetimes. This action is conformally related to the low-energy string action in three dimensions. The solution of the CDBH [30] is given by

$$ds^2 = -f(r)dt^2 + \frac{4r^2 dr^2}{\gamma^4 f(r)} + r^2 d^2\theta; \quad \phi = \frac{1}{4} \ln \left[ \frac{r}{\gamma^2} \right]; \quad F_{rt} = \frac{Q}{r^2},\tag{5}$$

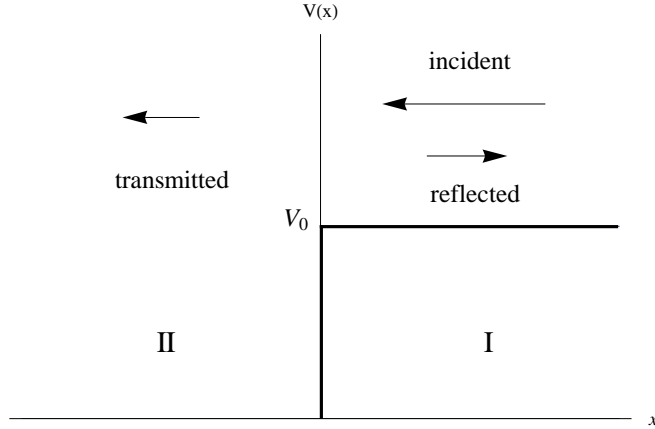


Figure 1: Potential-step: the incident wave comes from the right with  $E \geq V_0$

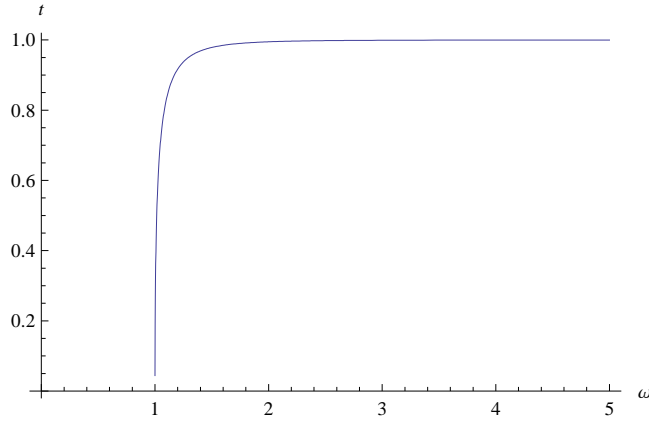


Figure 2: Transmission coefficient  $t$  for the potential-step: for  $m = 1/2$ ,  $\hbar = 1$ , and  $V_0 = 1$ . Note that  $\omega \geq 1$ .

where the metric function  $f(r) = -2Mr + 8\Lambda r^2 + 8Q^2$  and an integration constant  $\gamma$  with dimension  $[\text{L}]^{\frac{1}{2}}$  is necessary to have correct dimensions. Then, two horizons can be obtained from the condition of  $f(r) = 0$  as

$$r_{\pm} = \frac{M \pm \sqrt{M^2 - 64Q^2\Lambda}}{8\Lambda}, \quad (6)$$

where  $r_+$  ( $r_-$ ) is the outer (inner) horizon for  $M \geq 8Q\sqrt{\Lambda}$ . The degenerate horizon of  $r_e = r_+ = r_-$  appears when  $M = 8Q\sqrt{\Lambda}$ . The thermodynamics of CDBH will be discussed in Appendix.

In the background of the CDBH, we introduce a scalar perturbation  $\Phi$ , which satisfies the Klein-Gordon equation

$$(\nabla^2 - \mu^2)\Phi = 0. \quad (7)$$

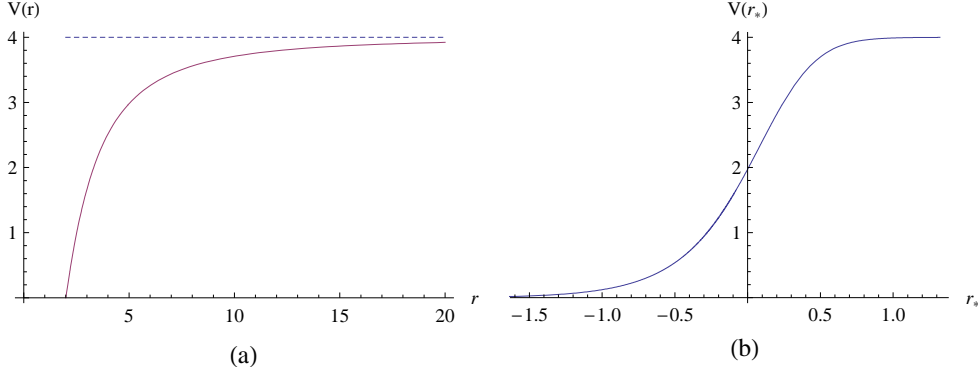


Figure 3: (a) The potential of the CDBH for  $M = 10$ ,  $Q = 1$ ,  $\Lambda = 1$ ,  $m = 0$ , and  $\gamma = 1$ . (b) The corresponding potential depicted in the tortoise coordinate  $r_*$ .

Hereafter we consider the massless case of  $\mu = 0$  only because the massive case gives rise to some difficulties with analytic calculations. Using the cylindrical symmetry of the background, let us parameterize  $\Phi$  as

$$\Phi(t, r, \theta) = e^{i\omega t} e^{im\theta} \xi(r). \quad (8)$$

Then, the above equation leads to the radial equation

$$\frac{d}{dr} \left( \frac{\gamma^4 f(r)}{2} \frac{d}{dr} \xi(r) \right) + 2r^2 \left( \frac{\omega^2}{f(r)} - \frac{m^2}{r^2} \right) \xi(r) = 0. \quad (9)$$

Redefining the radial function  $\xi(r)$  as

$$\xi(r) \equiv \frac{R(r)}{\sqrt{r}} \quad (10)$$

and introducing the tortoise coordinate defined by  $dr_* = 2rdr/\gamma^2 f(r)$ , the radial equation of the massless scalar perturbation becomes the Schrödinger equation with the energy  $E = \omega^2$

$$\left( \frac{d^2}{dr_*^2} + E - V(r) \right) R(r) = 0. \quad (11)$$

Here, the potential  $V(r)$  is given by

$$\begin{aligned} V(r) &= \gamma^4 \left( -\frac{12Q^4}{r^4} + \frac{4MQ^2}{r^3} - \frac{M^2}{4r^2} - \frac{8\Lambda Q^2}{r^2} + 4\Lambda^2 \right) \\ &+ \frac{m^2}{r^2} \left( -2Mr + 8\Lambda r^2 + 8Q^2 \right). \end{aligned} \quad (12)$$

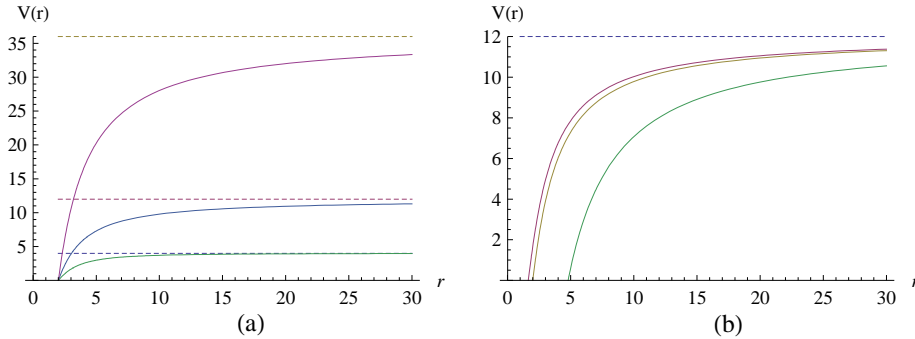


Figure 4: (a) The potentials for different angular momentum number  $m$  with  $M = 10$ ,  $Q = 1$ ,  $\Lambda = 1$ , and  $\gamma = 1$ . The curves are for  $m = 2$ ,  $m = 1$ , and  $m = 0$  from top to bottom, and start from the same  $r_+ = 2$ . (b) The potentials for different masses  $M$  with  $Q = 1$ ,  $\Lambda = 1$ ,  $m = 1$ , and  $\gamma = 1$ . The curves are for  $M = 9$  ( $r_+ = 1.6$ ),  $M = 10$  ( $r_+ = 2.0$ ), and  $M = 20$  ( $r_+ = 4.8$ ) from top to bottom. All curves approach the maximum  $V_0$  given by Eq. (13) as  $r$  increases.

This potential is depicted in Fig. 3(a). The potential is monotonically increasing outside the event horizon and approaching a constant value determined by the height of the potential step

$$V_0(m) = 8m^2\Lambda + 4\gamma^4\Lambda^2 \quad (13)$$

for a given  $m$ . On the other hand, for the CDBH case the tortoise coordinate takes the form

$$r_* = \frac{1}{4\gamma^2\Lambda(r_+ - r_-)} [r_+ \ln(r - r_+) - r_- \ln(r - r_-)]. \quad (14)$$

Then, when  $r \rightarrow r_+$ , the tortoise coordinate  $r_*$  approaches  $-\infty$ , while when  $r \rightarrow \infty$ , the tortoise coordinate  $r_*$  goes to  $\infty$ .

Now, in order to see the shape of the potential (12) expressed in terms of the tortoise coordinate  $r_*$ , let us draw the effective potential  $V(r_*)$  in Fig. 3(b) numerically. We observe from this graph that the effective potential is different from the Schwarzschild-type one, which has a shape of the barrier. For the CDBH, the shape of the potential is the step-type localized near  $r_* = 0$ , while for the Schwarzschild black hole, it looks like the barrier. Also we find similar graphs from Fig. 4 for different  $m$  and  $M$ .

From now on we separate the case of  $E > V_0$  from the case of  $E < V_0$  because the former has a completely different scattering picture from the latter. In order to compute the greybody factor and QNMs, we have to solve

the radial equation (9) completely by introducing a new coordinate

$$z = \frac{r - r_+}{r - r_-}, \quad (15)$$

which covers a compact region of  $0 \leq z \leq 1$ , corresponding to  $-\infty \leq r_* \leq \infty$  ( $r_+ \leq r \leq \infty$ ). Then, Eq. (9) leads to

$$z(1-z)R''(z) + (1-z)R'(z) + \frac{1}{\gamma^4}P(z)R(z) = 0, \quad (16)$$

where

$$P(z) = A + \frac{B}{z} + \frac{C}{z-1} \quad (17)$$

with

$$A = -\frac{r_-^2 \omega^2}{16\Lambda^2(r_+ - r_-)^2}, \quad B = \frac{r_+^2 \omega^2}{16\Lambda^2(r_+ - r_-)^2}, \quad C = \frac{\omega^2 - 8m^2\Lambda}{16\Lambda^2}. \quad (18)$$

With an ansatz of  $R(z) = z^\alpha(1-z)^\beta F(z)$ , the radial equation (16) is written by

$$z(1-z)F''(z) + [1 + 2\alpha - (1 + 2\alpha + 2\beta)z]F'(z) + \left( \frac{A}{\gamma^4} - (\alpha + \beta)^2 + \frac{B/\gamma^4 + \alpha^2}{z} + \frac{C/\gamma^4 + \beta^2 - \beta}{1-z} \right) F(z) = 0. \quad (19)$$

Comparing this with the hypergeometric equation [31] given by

$$z(1-z)\frac{d^2F}{dz^2} + [c - (1+a+b)z]\frac{dF}{dz} - abF = 0, \quad (20)$$

we have

$$c = 1 + 2\alpha, \quad (21)$$

$$a + b = 2\alpha + 2\beta, \quad (22)$$

$$ab = (\alpha + \beta)^2 - A/\gamma^4, \quad (23)$$

$$B/\gamma^4 + \alpha^2 = 0, \quad (24)$$

$$C/\gamma^4 + \beta^2 - \beta = 0. \quad (25)$$

By solving Eqs. (22) and (23), we have

$$a \equiv a_\pm = \alpha + \beta \pm \frac{\sqrt{A}}{\gamma^2}, \quad b \equiv b_\mp = \alpha + \beta \mp \frac{\sqrt{A}}{\gamma^2}, \quad (26)$$



respectively. One finds from Eqs. (24) and (25),

$$\alpha \equiv \alpha_{\pm} = \pm \frac{ir_+ \omega}{4\gamma^2 \Lambda (r_+ - r_-)}, \quad (27)$$

$$\beta \equiv \beta_{\pm} = \frac{1}{2} \left[ 1 \pm i \sqrt{\frac{\omega^2 - V_0}{4\gamma^4 \Lambda^2}} \right], \quad (28)$$

respectively. Hereafter we will use the upper signs of  $\alpha_+$  and  $\beta_+$  without loss of generality. For  $\omega^2 < V_0$ , we have a completely different case of  $\beta = \text{real}$ . This will be discussed in Sec. 4 separately. Since the hypergeometric equation (19) has regular singular points at  $z = 0$ ,  $z = 1$  and none of  $a$ ,  $b$ , and  $c$  are integer, there exists the general solution in the neighborhood of the points [31] such as  $C_1 F(a, b, c; z) + C_2 (1 - z)^{1-c} F(a - c + 1, b - c + 1, 2 - c; z)$  with two unknown constants  $C_1$  and  $C_2$ .

Now, in order to find the scattering picture of a massless scalar on the CDBH, we need to specify boundary conditions: near horizon and at infinity. We choose the condition that the wave is purely ingoing ( $\leftarrow$ ) near the horizon. Then, we find the ingoing mode (transmitted mode) near  $z = 0$  by choosing  $C_2 = 0$  as

$$e^{i\omega t} R(r_* \rightarrow -\infty) = \frac{C_1}{|r_+ - r_-|^{\alpha}} e^{i\omega(t+r_*)}. \quad (29)$$

On the other hand, the asymptotic solution matched with Eq. (29) is

$$\begin{aligned} e^{i\omega t} R(r_* \rightarrow \infty) &= D_1 e^{i\omega \left( t - r_* \sqrt{1 - \frac{V_0}{\omega^2}} \right) - 2\gamma^2 \Lambda r_*} \\ &+ D_2 e^{i\omega \left( t + r_* \sqrt{1 - \frac{V_0}{\omega^2}} \right) - 2\gamma^2 \Lambda r_*}, \end{aligned} \quad (30)$$

where  $D_1, D_2$  are defined by

$$\begin{aligned} D_1 &= C_1 \left( \frac{r_+ - r_-}{r_+} \right)^{\beta} \frac{\Gamma(1 + 2\alpha) \Gamma(1 - 2\beta)}{\Gamma(1 + \alpha - \beta - \sqrt{A}/\gamma^2) \Gamma(1 + \alpha - \beta + \sqrt{A}/\gamma^2)}, \\ D_2 &= C_1 \left( \frac{r_+ - r_-}{r_+} \right)^{1-\beta} \frac{\Gamma(1 + 2\alpha) \Gamma(2\beta - 1)}{\Gamma(\alpha + \beta + \sqrt{A}/\gamma^2) \Gamma(\alpha + \beta - \sqrt{A}/\gamma^2)}, \end{aligned} \quad (31)$$

respectively. Note that the first  $D_1$  term in Eq. (30) is an outgoing mode ( $\rightarrow$ ) and the second  $D_2$  term is an ingoing mode ( $\leftarrow$ ) at infinity.

Using these solutions, one can calculate the partial wave absorption cross section as

$$\sigma(\omega, m) = \frac{1}{\omega} \left| \frac{\mathcal{F}_{tr}(r \rightarrow r_+)}{\mathcal{F}_{in}(r \rightarrow \infty)} \right| = \frac{8\pi r_+ |C_1|^2 / \gamma^2}{16\pi |D_2|^2 (r_+ - r_-) \Lambda \sqrt{\frac{V_0 - \omega^2}{4\gamma^4 \Lambda^2}}} \quad (32)$$

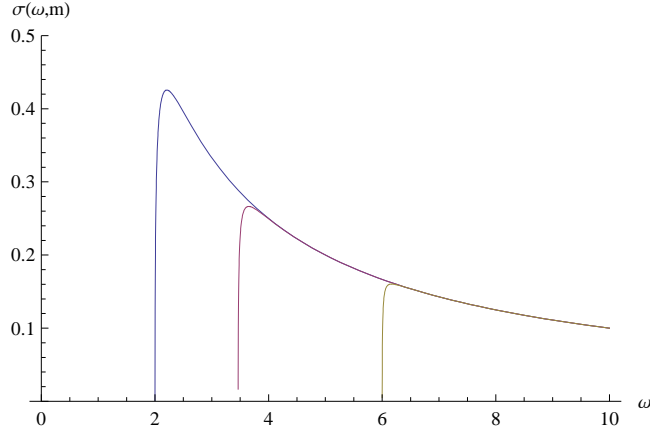


Figure 5: Plots of the partial wave absorption cross section for  $M = 10$ ,  $Q = 1$ ,  $\Lambda$ , and  $\gamma = 1$ : the curves are depicted for  $m = 0$ ,  $m = 1$ , and  $m = 2$  from left to right.

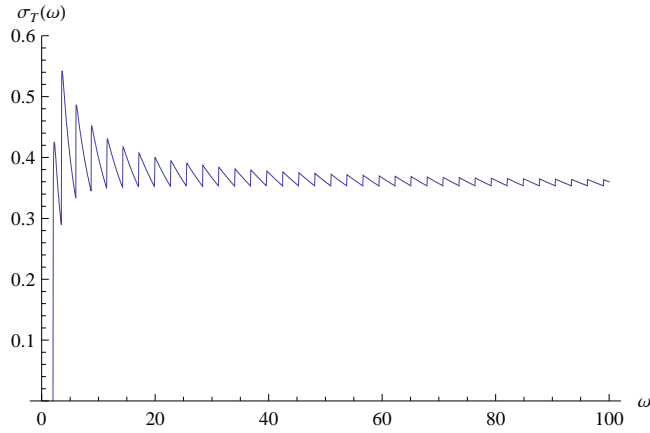


Figure 6: Plot of total absorption cross section for  $M = 10$ ,  $Q = 1$ ,  $\Lambda = 1$ , and  $\gamma = 1$ . It is obtained by summing  $\sigma(\omega, m)$  from  $m = 0$  to  $m = 35$ .

$$= \frac{\gamma^2 \sinh\left(\frac{\pi\omega r_+}{2\gamma^4\Lambda^2}\right) \sinh\left(\pi\sqrt{\frac{\omega^2 - V_0}{4\gamma^4\Lambda^2}}\right)}{\omega \cosh\left(\frac{\pi}{2}\sqrt{\frac{\omega^2 - V_0}{4\gamma^4\Lambda^2}} + \frac{\pi\omega}{4\gamma^2\Lambda}\right) \cosh\left(\frac{\pi}{2}\sqrt{\frac{\omega^2 - V_0}{4\gamma^4\Lambda^2}} + \frac{\pi\omega(r_+ + r_-)}{4\gamma^2\Lambda(r_+ - r_-)}\right)},$$

which is depicted for  $m = 0, 1, 2$  in Fig. 5. We confirm that  $\sigma(\omega = \sqrt{V_0}, m) = 0$ , which shows no transmission clearly. This contrasts to the case of the Schwarzschild black hole, which shows the universal behavior of  $\sigma^{SBH}(\omega \rightarrow 0) \rightarrow \mathcal{A}_H$  with the area of horizon  $\mathcal{A}_H$  for a massless scalar propagation.

On the other hand, the total absorption cross section given by

$$\sigma_T(\omega) = \sum_m \sigma(\omega, m) \quad (33)$$

is depicted in Fig. 6. Note that the maximum of each partial absorption cross section makes a local maximum in the total absorption cross section. As  $\omega$  increases,  $\sigma_T$  approaches a constant value,  $2\pi/17 = 0.37$ . This oscillatory behavior in the total absorption cross section reflects the wiggly characteristic of the potential-steps surrounding the CDBH. Note that similar oscillatory behavior also appear in the total absorption cross sections of the Schwarzschild black hole [32, 33] and the  $D3$ -brane [34].

In the case of the potential-barriers surrounding the Schwarzschild black hole, the total cross section is given by [32]

$$\sigma_T^{SBH}(\omega) = \frac{27\pi}{4} - \frac{\sqrt{2}\sin(\sqrt{2\pi^3}\omega)}{\omega} \quad (34)$$

which indicates the limiting value of  $27\pi/4 = 21.2$  for large  $\omega$ . Hence, the high energy limit ( $\omega \gg \sqrt{V_0}$ ) of the total cross section of the CDBHs is also similar to the case of the Schwarzschild black hole, even though the latter shows the potential-barriers with different heights for different angular momentum number  $\ell$ . However, for the CDBH case the low energy limit of  $\omega \rightarrow \sqrt{V_0}$  is quite different from the case of the Schwarzschild black hole.

### 2.3 The Schwarzschild-AdS black holes (SAdS)

It was reported that the electromagnetic perturbations on the SAdS space-time shows the purely imaginary QNM frequencies [13]. Let us study the propagation of an electromagnetic field in the SAdS with the line element

$$ds^2 = -f(r)dt^2 + \frac{dr^2}{f(r)} + r^2 d^2\Omega, \quad (35)$$

where  $f(r) = 1 - 2M/r + r^2/R^2$  and  $R$  is the AdS radius. An electromagnetic wave on this background is described by Maxwell equation, which turns out to be the Schrödinger-like equation of the type (11) for the radial part. The general form is given by

$$\frac{d^2\psi}{dr_*^2} + [\omega^2 - V_{SAdS}(r)]\psi = 0, \quad (36)$$

where the potential is given by

$$V_{SAdS}(r) = f(r) \left[ \frac{l(l+1)}{r^2} + \frac{\beta}{r^3} \right]. \quad (37)$$

Here  $\beta$  is  $-6M$ ,  $0$ , and  $2M$  for odd-gravitational, electromagnetic and scalar perturbations, respectively. For the  $\beta = 0$  case, its shape is depicted in

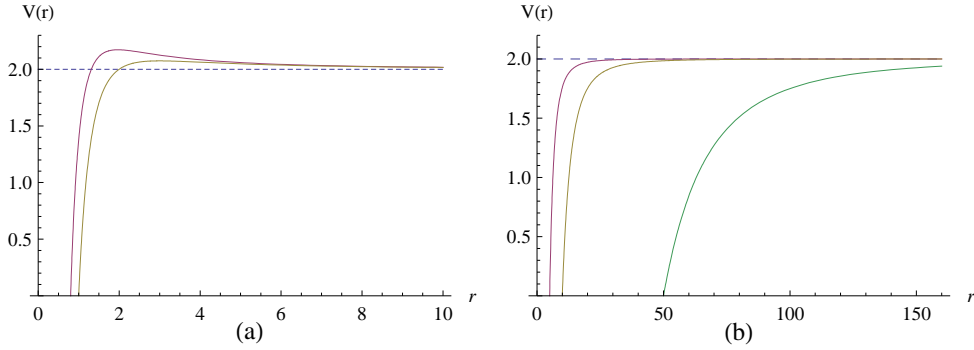


Figure 7: Two different types of potentials for the SAdS black holes with  $R = 1$ ,  $l = 1$ . (a) The barrier-type for small black holes with  $r_+ < 5$ : Two curves from left to right are for  $M = 0.656$  ( $r_+ = 0.8$ ) and  $M = 1$  ( $r_+ = 1$ ), which have a bump rising above the asymptotic value of the potential  $V_{0SAdS} = 2$ . (b) The step-type for large black holes with  $r_+ \geq 5$ : Three curves under  $V_{0SAdS} = 2$  are for  $M = 65$  ( $r_+ = 5$ ),  $M = 505$  ( $r_+ = 10$ ), and  $M = 62505$  ( $r_+ = 50$ ) from left to right.

Fig. 7. As shown in this figure, the potential for a large SAdS black hole approaches a constant value given by  $V_{0SAdS} = l(l+1)/R^2$  of a step-type, while in the Schwarzschild limit ( $R \rightarrow \infty$ ), its asymptotic tail goes to zero, making a barrier-type potential. Note here that there exists a local bump near the horizon, depending the mass of the black hole. For the small black hole with  $r_+ < 5$ , the potential has the maximum value near the horizon, while for the large black hole with  $r_+ > 5$ , the maximum disappears and its shape becomes the potential-step. This is similar to the massless scalar perturbation on the CDBH in the previous section.

### 3 Quasinormal modes

In general, the QNMs can be decomposed into real and imaginary parts as follows:

$$\omega = \omega_r - i\omega_i. \quad (38)$$

In this section, we provides two cases of purely damped modes with  $\omega_r = 0$ . We explore the connection between the purely imaginary QNMs and the potential-steps surrounding the black holes.

Numerical Results		
$r_+$	$-\omega_i$	$\omega_r$
0.8	1.287	2.175
1	1.699	2.163
5	8.795	$\sim 0$
10	15.506	$\sim 0$
50	75.096	$\sim 0$
100	150.048	$\sim 0$

Table 1: In the case of  $l = 1$ , the QNMs frequencies of electromagnetic perturbation for selected values of  $r_+$  on the SAdS.

### 3.1 QNMs in the SAdS

It is by now well-known that the electromagnetic perturbation on the SAdS shows the different feature that its QNMs take purely imaginary values for a large black hole [13]. Here we quote their results in Table 1 that shows the lowest QNMs for the  $l = 1$  electromagnetic perturbation on the SAdS spacetime.

We observe that starting from  $r_+ = 5$ , they have imaginary values. Note that for the small black holes with  $r_+ < 5$ , the shape of potential is the barrier-type. See Fig. 7(a). On the other hand, for the large black holes with  $r_+ \geq 5$ , as shown in Fig. 7(b), the corresponding potentials are the step-type. In order to have complex QNMs, the potential should have a bump (local maximum) somewhere. The presence of bump near the horizon explains clearly why the QNMs of the small Schwarzschild-AdS black hole are complex [13].

### 3.2 QNMs in the CDBH

The QNMs are the solutions of the wave equation characterized by purely ingoing waves near the horizon. In addition, one has to impose the boundary condition at infinity. Thus, one needs to know the asymptotic geometry of the spacetime under study, which is provided by the potential. As for the CDBH, the author [27, 28] took the boundary condition for the asymptotic region as the AdS spacetime. However, as seen from the potential in Fig. 3(a) and 3(b), the energy of a perturbed scalar should be higher than the maximum effective potential  $V_0$  for  $E > V_0$ . On the other hand, the propagating wave could not be developed for  $E < V_0$ . Thus, a boundary condition for the CDBH seems to be the one in asymptotically flat spacetime: purely outgoing

waves at infinity [12]. Precisely, as is shown in Eq. (30), it is a combination of asymptotically flat spacetimes (plane waves) and AdS spacetimes ( $e^{-2\gamma^2\Lambda r_-}$ -normalizable mode).

Considering the asymptotic solution Eq. (30), keeping the first term ( $D_1 \neq 0, D_2 = 0$ ) corresponds to the outgoing mode only. Equivalently, considering the scattering resonances at the pole of the transmission amplitude ( $D_2 \rightarrow 0$ ) leads to the condition for QNMs for the massless scalar on the CDBH as

$$\alpha + \beta \pm \frac{\sqrt{A}}{\gamma^2} = -n \quad (39)$$

with the positive integer  $n$ . From this condition, we obtain the quasinormal frequencies

$$\begin{aligned} \omega_n &= -i \frac{\gamma^2 \Lambda (r_+ - r_-)}{2r_+ r_-} \left[ (2n+1)(r_+ + r_-) \right. \\ &\quad \left. + \sqrt{(2n+1)^2 (r_+ + r_-)^2 - 16n(n+1)r_+ r_- + \frac{8m^2 r_+ r_-}{\gamma^4 \Lambda}} \right] \quad (40) \\ &= -i \frac{\pi T_H}{2} \left[ (2n+1) \left( 1 + \frac{r_+}{r_-} \right) \right. \\ &\quad \left. + \sqrt{(2n+1)^2 \left( 1 + \frac{r_+}{r_-} \right)^2 - 16n(n+1)r_+ + \frac{8m^2 r_+}{\gamma^4 \Lambda}} \right], \quad (41) \end{aligned}$$

where the Hawking temperature is given by  $T_H = \gamma^2 \Lambda (r_+ - r_-) / \pi r_+$ . We prove that  $\omega_n$  is purely imaginary by numerically showing that the quantity inside the square root is always positive for any CDBH.

## 4 $E < V_0$ case in the CDBH

This case corresponds to the purely real  $\beta$  case and in turn its flux becomes zero. Let us explain this situation by introducing a wave propagation from left to right under a potential-step with height  $V_0 (> E = \omega^2)$  in Fig. 1. Since the density of incident wave is unity, its flux ( $\mathcal{F}_{IIin}$ ) is equal to  $2\omega$ . The reflected flux  $\mathcal{F}_{IIre}$  is given by  $-2\omega$  and thus there is no net flux in region II:  $\mathcal{F}_{IIin} + \mathcal{F}_{IIre} = 0$ . According to the flux conservation, we expect that there is no flux in region I. As a check, one finds that  $\mathcal{F}_I = \frac{1}{i} [\Psi_I^* (\Psi_I)' - \Psi_I (\Psi_I^*)'] = 0$ . Even though the probability density of finding a particle between  $x$  and  $x + dx (x > 0)$  is not zero, its flux is zero. This means that the quantum mechanical picture reduces to the classical picture of the total reflection. A plane wave moving under a potential-step with the height

$V_0(> E)$  corresponds to a toy model for the total reflection with  $|R|^2 = 1$  and  $R = e^{-2i\theta}$  (non-zero phase). A similar situation occurs in a scalar wave propagating under de Sitter space [29].

In this case we have no absorption cross section of  $\sigma(\omega, m) = \mathcal{F}_I/\omega\mathcal{F}_{Ire} = 0$  because of zero flux  $\mathcal{F}_I = 0$ . Furthermore, QNMs are not defined since we could not make  $\mathcal{F}_{Iin} = 0$  without  $\mathcal{F}_{Ire} = 0$ . This result is consistent with the picture of stable event horizon because the presence of quasinormal frequencies implies that the massless scalar wave is losing its energy continuously into the event horizon. This means that the event horizon is usually stable and it is always in thermal equilibrium with the scalar perturbation. More explicitly, the event horizon not only absorbs scalar waves but also emits those previously absorbed by itself at the same rate. As a result, the case of  $E < V_0$  corresponds to a forbidden region for scattering (absorption cross section) and scattering resonances (QNMs).

## 5 Discussions

We clarify the purely imaginary quasinormal frequencies of a massless scalar perturbation on the 3D charged-dilaton black holes(CDBH) using the scattering (resonance) picture for  $E > V_0$  with the energy  $E = \omega^2$  and the height  $V_0$  of the potential step. In fact, the purely imaginary quasinormal frequencies represent a special set of modes which are purely damped [16]. These are not regular QNMs because the real part of frequencies vanishes, eliminating the oscillatory behavior of the perturbations which is characteristic of QNMs.

This CDBH case is quite interesting because we have found the potential-steps outside the event horizon, similar to the case of the electromagnetic and odd-gravitational perturbations on the large Schwarzschild-AdS black holes. We believe that the potential surrounding the black hole provides all information to a perturbation field propagating on the black hole background.

Moreover, we have shown that the potential-step type provides the purely imaginary quasinormal frequencies, while the potential-barrier type gives the complex quasinormal frequencies. For  $E < V_0$ , which is the case of de Sitter space, we could not find any QNMs.

Finally, we discuss the connection between thermodynamics of black hole and QNMs. As is shown in Appendix, we have shown that thermodynamics of the CDBH has a new feature comparing with the non-rotating BTZ black hole, which provides the complex QNMs. This includes a constant value of temperature and different behaviors of mass and heat capacity for the large CDBH. Even though thermodynamics of the CDBH is different from that of

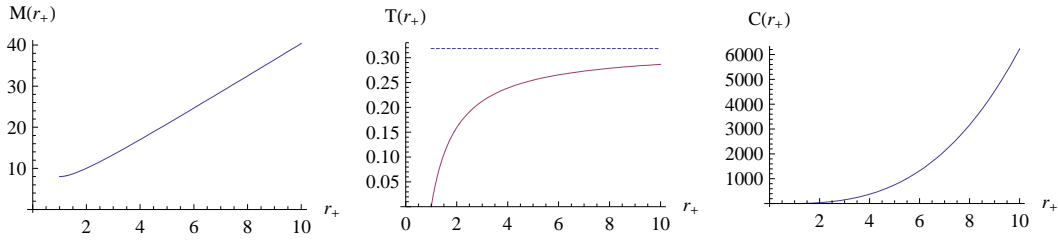


Figure 8: Graphs of mass, temperature, and specific heat of the CDBH for  $Q = 1$ ,  $\Lambda = 1$ , and  $\gamma = 1$ , respectively.

the non-rotating BTZ black hole, it is not clear why the QNMs of the CDBH are purely imaginary whereas the QNMs of the non-rotating BTZ black hole are complex. However, comparing their potentials leads to the fact that the potentials of the CDBH are step-type, while those of the non-rotating BTZ black hole are monotonically increasing functions. The latter are infinite at infinity [35].

Consequently, we have shown that the purely imaginary quasinormal frequencies of a massless scalar is determined by its potential-steps surrounding the charged-dilaton black hole.

## Appendix: Thermodynamics of the CDBH

In this Appendix, we consider the thermodynamic quantities of the CDBH.

The mass of the CDBH is given by

$$M(r_+, Q, \Lambda) = 4\Lambda r_+ \left( 1 + \frac{Q^2}{\Lambda r_+^2} \right). \quad (42)$$

For large black hole, it is given by  $M \propto 4\Lambda r_+$ .

The Hawking temperature is

$$T(r_+, Q, \Lambda) = \frac{\gamma^2 \Lambda}{\pi} \left( 1 - \frac{Q^2}{\Lambda r_+^2} \right). \quad (43)$$

For the large black hole, the temperature goes to a constant value of  $\gamma^2 \Lambda / \pi$ , which is the temperature of the uncharged-dilaton black hole. This is a new feature of the CDBH.

The specific heat is

$$C(r_+, Q, \Lambda) = \frac{2\pi \Lambda r_+^3}{Q^2} \left( 1 - \frac{Q^2}{\Lambda r_+^2} \right). \quad (44)$$



The heat capacity has a single positive phase like the non-rotating BTZ black hole but there exists a difference in their forms. Note that the thermodynamic quantities of the non-rotating BTZ black hole are given by  $M_{NBTZ} = \Lambda r_+^2$ ,  $T_{NBTZ} = \Lambda r_+/2\pi$ ,  $C_{NBTZ} = S_{NBTZ} = 4\pi r_+$  with  $\Lambda = 1/l^2$ . The extremal mass  $M_e$  is given by  $8Q\sqrt{\Lambda}$  at the degenerate horizon  $r_e = Q/\sqrt{\Lambda}$ , where the temperature and specific heat vanish.

Finally, the Bekenstein-Hawking entropy is given by the area-law as

$$S_{BH} = \frac{2\pi r_+}{4G} = 4\pi r_+ \quad (45)$$

with  $G = 1/8$ . Then, we can easily check that the first-law of thermodynamics is satisfied as

$$\gamma^2 dM = T dS_{BH}. \quad (46)$$

## Acknowledgment

Two of us (Y. S. Myung and Y.-J. Park) were supported by the Science Research Center Program of the Korea Science and Engineering Foundation through the Center for Quantum Spacetime of Sogang University with grant number R11-2005-021. Y.-W. Kim was supported by the Korea Research Foundation Grant funded by Korea Government (MOEHRD): KRF-2007-359-C00007.

## References

- [1] R. Ruffini and J. A. Wheeler, *Physics Today* **24**, 30 (1971).
- [2] C. V. Vishveshwara, *Nature*, **227**, 936 (1970).
- [3] W. H. Press, *Astrophys. J.* **170**, L105 (1971).
- [4] T. Regge, *Phys. Rev.* **108**, 1063 (1957).
- [5] F. J. Zerilli, *Phys. Rev. Lett.* **24**, 737 (1970).
- [6] C. V. Vishveshwara, *Phys. Rev. D* **1**, 2870 (1970).
- [7] S. Chandrasekhar, *in The mathematical Theory of Black Holes* (Oxford Univ., New York, 1983).

- [8] O. J. Kwon, Y. D. Kim, Y. S. Myung, B. H. Cho and Y. J. Park, Phys. Rev. D **34**, 333 (1986).
- [9] S. Hod, Phys. Lett. B **666**, 483 (2008).
- [10] K. D. Kokkotas and B. G. Schmidt, Living Rev. Rel. **2**, 2 (1999) [arXiv:gr-qc/9909058].
- [11] O. Aharony, S. S. Gubser, J. M. Maldacena, H. Ooguri and Y. Oz, Phys. Rept. **323**, 183 (2000) [arXiv:hep-th/9905111].
- [12] G. T. Horowitz and V. E. Hubeny, Phys. Rev. D **62**, 024027 (2000) [arXiv:hep-th/9909056].
- [13] V. Cardoso and J. P. S. Lemos, Phys. Rev. D **64**, 084017 (2001) [arXiv:gr-qc/0105103].
- [14] I. G. Moss and J. P. Norman, Class. Quant. Grav. **19**, 2323 (2002) [arXiv:gr-qc/0201016].
- [15] B. Wang, C. Y. Lin and E. Abdalla, Phys. Lett. B **481**, 79 (2000) [arXiv:hep-th/0003295].
- [16] A. S. Miranda, J. Morgan and V. T. Zanchin, [arXiv:0809.0297 [hep-th]].
- [17] R. Aros, C. Martinez, R. Troncoso and J. Zanelli, Phys. Rev. D **67**, 044014 (2003) [arXiv:hep-th/0211024].
- [18] D. Birmingham and S. Mokhtari, Phys. Rev. D **74**, 084026 (2006) [arXiv:hep-th/0609028].
- [19] A. Lopez-Ortega, Gen. Rel. Grav. **39**, 1011 (2007) [arXiv:0704.2468 [gr-qc]].
- [20] A. Lopez-Ortega, Gen. Rel. Grav. **38**, 1565 (2006) [arXiv:gr-qc/0605027].
- [21] M. Banados, C. Teitelboim and J. Zanelli, Phys. Rev. Lett. **69**, 1849 (1992) [arXiv:hep-th/9204099];  
M. Banados, M. Henneaux, C. Teitelboim and J. Zanelli, Phys. Rev. D **48**, 1506 (1993) [arXiv:gr-qc/9302012].
- [22] D. Birmingham, Phys. Rev. D **64**, 064024 (2001) [arXiv:hep-th/0101194].

- [23] D. Birmingham, I. Sachs and S. N. Solodukhin, Phys. Rev. Lett. **88**, 151301 (2002) [arXiv:hep-th/0112055].
- [24] V. Cardoso and J. P. S. Lemos, Phys. Rev. D **63**, 124015 (2001) [arXiv:gr-qc/0101052].
- [25] E. Abdalla, B. Wang, A. Lima-Santos, and W. G. Qiu, Phys. Lett. B **538**, 435 (2002) [arXiv:hep-th/0204030].
- [26] S. Fernando, Gen. Rel. Grav. **36**, 71 (2004) [arXiv:hep-th/0306214].
- [27] S. Fernando, Gen. Rel. Grav. **37**, 461 (2005) [arXiv:hep-th/0407163].
- [28] S. Fernando, Phys. Rev. D **77**, 124005 (2008) [arXiv:0802.3321 [hep-th]].
- [29] Y. S. Myung and N. J. Kim, Class. Quant. Grav. **21**, 63 (2004) [arXiv:hep-th/0304231].
- [30] K. C. K. Chan and R. B. Mann, Phys. Rev. D **50**, 6385 (1994) [Erratum-ibid. D **52**, 2600 (1995)] [arXiv:gr-qc/9404040].
- [31] M. Abramowitz and I. A. Stegun, *Handbook of Mathematical Functions*, Dover, New York, 1965.
- [32] N. G. Sanchez, Phys. Rev. D **18**, 1030 (1978).
- [33] E. Jung and D. K. Park, Class. Quant. Grav. **21**, 3717 (2004) [arXiv:hep-th/0403251].
- [34] M. Cvetič, H. Lu and J. F. Vazquez-Poritz, JHEP **0102**, 012 (2001) [arXiv:hep-th/0002128].
- [35] Y. S. Myung and H. W. Lee, Mod. Phys. Lett. A **21**, 1737 (2006) [arXiv:hep-th/0506031].